PORTABLE POWER GENERATION VIA INTEGRATED CATALYTIC MICROCOMBUSTION-THERMOELECTRIC DEVICES

D. G. Norton, K. W. Voit, T. Brüggemann, and D. G. Vlachos
University of Delaware, Dept. of Chemical Engineering and Center for Composite Materials
Newark, DE 19716-3110

E. D. Wetzel
Army Research Laboratory, Weapons and Materials Research Directorate
Aberdeen Proving Ground, Maryland 21005-5069

ABSTRACT

U.S. Army systems increasingly require novel methods of high density, fast charging power sources. In this study, a novel alternative to traditional batteries, catalytic microcombustors utilizing hydrocarbon fuels, are fabricated and characterized. These devices are found to be robust, easy to start up, operable over a wide range of compositions and temperatures, and able to support complete combustion over a range of fuels and fuel/air ratios. Various materials of construction are investigated in order to yield good temperature uniformity. Successful integration with thermoelectric devices is achieved, resulting in electrical power generation from catalytic microcombustion with a thermal efficiency of ~1%.

1. INTRODUCTION

Advances in soldier technology have led to the proliferation of portable electronic devices on the battlefield, including communication equipment, global positioning systems, night vision goggles, and chem-bio agent detectors. Additionally, new miniature vehicles, such as mules and mini-unarmed aerial vehicles, as well as instrumented munitions, are also being fielded. All of these systems require compact power systems that are safe, light, efficient, and robust.

Traditional batteries have a low energy density, which places burdensome weight and power limitations on system design. Furthermore, the highest energy density batteries are often non-rechargeable. These single-use batteries necessarily produce significant economic, logistic, and environmental burdens.

Power generation utilizing hydrocarbons offers a promising alternative to traditional batteries. The energy density of hydrocarbons is significantly higher than that of batteries (approximately 40 vs. 0.5 MJ/kg for lithium-ion battery chemistries) (Sitzki et al., 2001). A hydrocarbon-based device with an overall efficiency of approximately 1% or greater can therefore lead to improvements over current battery technology. Furthermore, hydrocarbon-based power systems can be quickly "recharged" simply by physical addition of more fuel.

Proton exchange membrane (PEM)-based fuel cells convert hydrogen directly into electricity. However, systems utilizing compressed H_2 produce low system-level energy density because of the high strength tanks required to store the gas at high pressures, and prevention of explosions is a major concern. Direct methanol fuel cells (DMFCs) suffer from crossover of methanol from the anode to the cathode, which depresses the cell voltage and results in fuel loss (Patil et al., 2004). System energy density is also reduced, since most DMFC devices require significant aqueous dilution of the methanol fuel.

Recent efforts have attempted to utilize combustion of hydrocarbons in miniature devices to directly produce heat or power (Ahn et al., 2003). These devices typically utilize conventional homogeneous (gas-phase) combustion, the same processes by which macroscopic flames produce heat. A major disadvantage of homogeneous combustion is that operating temperatures are necessarily very high (>1500ºC). These high temperatures greatly limit material selection, require extensive combustor insulation, and lead to significant NO_x production (Miller et al., 1989). Thermal management is not only critical for system compatibility with electronics, packaging, and personnel, but also for control of thermal signature. Furthermore, some of these devices consist of complicated miniature parts, which are difficult and expensive to fabricate, and so far have exhibited efficiencies well below 1% (Schaevitz et al., 2001).

An alternative to homogeneous microcombustion is to combust the fuel catalytically, without the production of a flame. When implemented in miniature devices, catalytic microcombustion has the potential to fully utilize the high energy densities of hydrocarbon fuels, but at much lower operating temperatures. Additionally, catalytic systems are typically easier to start (could in fact

Report Documentation Page		*Form Approved* *OMB No. 0704-0188*

Public reporting burden for the collection of information is estimated to average 1 hour per response, including the time for reviewing instructions, searching existing data sources, gathering and maintaining the data needed, and completing and reviewing the collection of information. Send comments regarding this burden estimate or any other aspect of this collection of information, including suggestions for reducing this burden, to Washington Headquarters Services, Directorate for Information Operations and Reports, 1215 Jefferson Davis Highway, Suite 1204, Arlington VA 22202-4302. Respondents should be aware that notwithstanding any other provision of law, no person shall be subject to a penalty for failing to comply with a collection of information if it does not display a currently valid OMB control number.

1. REPORT DATE **00 DEC 2004**	2. REPORT TYPE **N/A**	3. DATES COVERED **-**	
4. TITLE AND SUBTITLE **Portable Power Generation Via Integrated Catalytic Microcombustion-Thermoelectric Devices**		5a. CONTRACT NUMBER	
		5b. GRANT NUMBER	
		5c. PROGRAM ELEMENT NUMBER	
6. AUTHOR(S)		5d. PROJECT NUMBER	
		5e. TASK NUMBER	
		5f. WORK UNIT NUMBER	
7. PERFORMING ORGANIZATION NAME(S) AND ADDRESS(ES) **University of Delaware, Dept. of Chemical Engineering and Center for Composite Materials Newark, DE 19716-3110; Army Research Laboratory, Weapons and Materials Research Directorate Aberdeen Proving Ground, Maryland 21005-5069**		8. PERFORMING ORGANIZATION REPORT NUMBER	
9. SPONSORING/MONITORING AGENCY NAME(S) AND ADDRESS(ES)		10. SPONSOR/MONITOR'S ACRONYM(S)	
		11. SPONSOR/MONITOR'S REPORT NUMBER(S)	
12. DISTRIBUTION/AVAILABILITY STATEMENT **Approved for public release, distribution unlimited**			
13. SUPPLEMENTARY NOTES **See also ADM001736, Proceedings for the Army Science Conference (24th) Held on 29 November - 2 December 2005 in Orlando, Florida. , The original document contains color images.**			
14. ABSTRACT			
15. SUBJECT TERMS			

16. SECURITY CLASSIFICATION OF:			17. LIMITATION OF ABSTRACT **UU**	18. NUMBER OF PAGES **8**	19a. NAME OF RESPONSIBLE PERSON
a. REPORT **unclassified**	b. ABSTRACT **unclassified**	c. THIS PAGE **unclassified**			

Standard Form 298 (Rev. 8-98)
Prescribed by ANSI Std Z39-18

be self-igniting (Norton et al., 2004)), more robust to heat losses, and self-sustained at leaner fuel/air ratios.
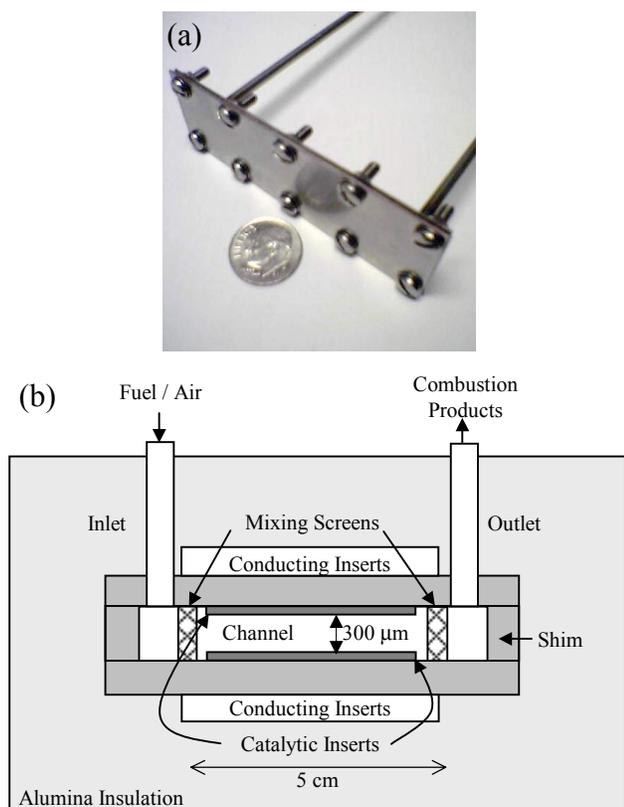

Figure 1. (a) Photograph of a microcombustor (small microcombustor; see experimental section) and (b) schematic of side view of the microcombustors (not to scale for ease of visualization

In our previous work, ceramic catalytic microcombustors were fabricated and tested (Norton and Vlachos, 2004; Norton et al., 2004). Hydrogen/air mixtures were found to be self-igniting and self-sustaining down to the leanest possible compositions. When the gap size, i.e., the characteristic microcombustor dimension, was reduced below 1 mm, homogeneous combustion was eliminated. Propane/air mixtures were found to be self-sustaining over a wide range of compositions, at gap sizes as small as 250 μm examined experimentally, and the self-igniting nature of hydrogen was used to start propane/air mixtures without any ignition sources. Elimination of ignition sources is an important finding because it reduces device size and weight. Finally, complete fuel conversion was observed over a wide range of conditions, an essential feature for device efficiency, safety, and environmental impact. Key to this high performance is the enhanced transport rates achieved at the microscale. However, these initial microcombustors produced thermal energy only, exhibited large temperature non-uniformity, and were not capable of generating usable electrical power.

In this paper, we demonstrate a second-generation of catalytic microcombustion-based devices. The bulky ceramic walls of the previous devices have been replaced by metal components with integrated insulation layers, resulting in a more compact and rugged device. Additional thermal diffusion layers are added to the combustion device to reduce thermal gradients along the combustion zone. Finally, the microcombustor is directly coupled to a thermoelectric device, demonstrating thermal efficiencies of ~ 1% and the operation of a commercial electronic device from both hydrogen and propane fuel sources. These microcombustors are shown in Figures 1 and 2a.
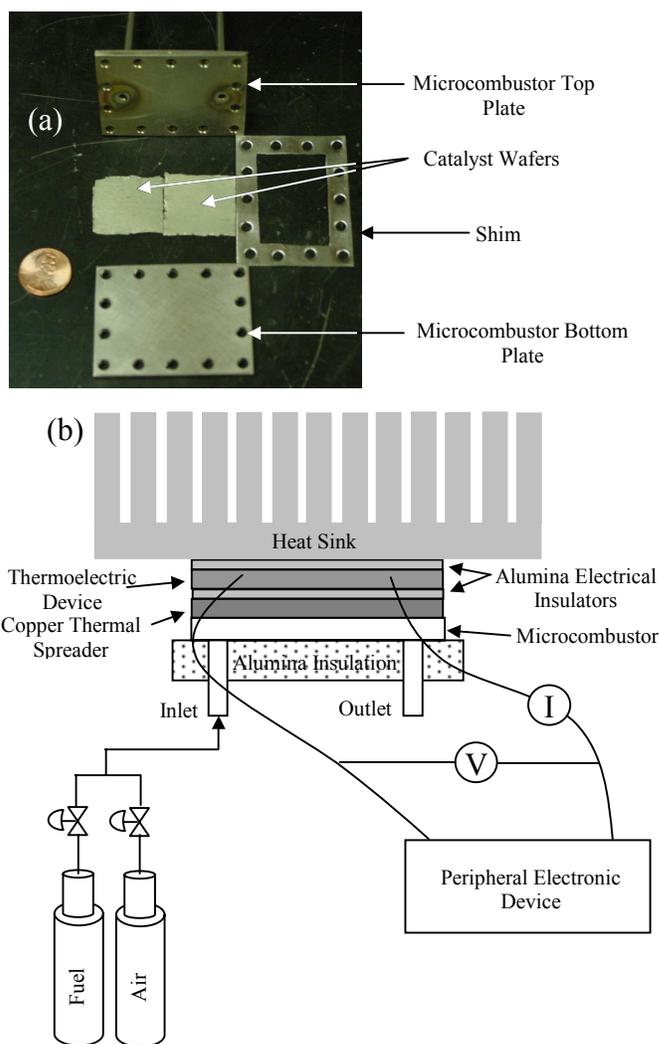

Figure 2. (a) Photograph of a disassembled microcombustor (large microcombustor; see experimental section) that is used for electricity generation. (b) Schematic of the thermoelectric-microcombustor device showing the major device components (not to scale).

2. EXPERIMENTAL APPARATUS

Two sets of microcombustors were fabricated for this study, both of which follow the schematic of Figure 1b. The combustion chamber consists of a thin stainless steel gasket sandwiched between two thicker stainless steel plates. The thickness of the stainless steel gasket was 500 μm in all cases. Stainless steel inlet and outlet tubes are welded to the top plate, at opposite ends of the combustion zone. Fine metal screens are placed at the entrance and exit of the combustion zone to act as static mixers, promoting uniform flow over the entire length of the catalyst, and preventing "jetting" of the reactants (Norton et al., 2004). Catalyst is deposited on thin alumina inserts, which are separated in the combustion chamber by 1-mm-wide alumina shims to create a total channel height of 300 μm. Holes spaced along the periphery of the top and bottom plates allow the assembly to be bolted together. Conducting wall inserts are affixed to the outer walls of the burner using silver paste, in order to systematically vary the axial thermal conductivity of the combustion zone walls (see Figures 1b and 2b). The entire burner is enclosed in an insulating, 6.4-mm-thick fibrous alumina jacket.
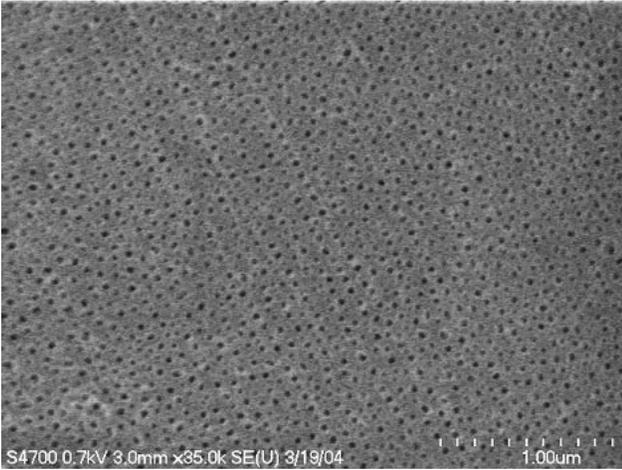

Figure 3. Scanning electron micrograph of the porous structure of the anodized alumina wafer. The pores have diameters on the order of 50 nm.

The first microcombustor (see Figure 1a), which we will refer to as the small microcombustor, was fabricated primarily to characterize system performance and optimize materials selection. The top and bottom plates are 0.79 mm thick, and the combustion zone (inner dimension of the stainless steel gasket) is 1 cm wide by 5 cm long. The resulting burner volume is ~142 μL. The second microcombustor (see Figure 2a), which we will refer to as the large microcombustor, is wider, with a combustion zone 3 cm wide by 5 cm long. The resulting burner volume for this device is ~349 μL. This larger area is designed to fit the form factor of the thermoelectric device. Additionally, the increased channel width allows for larger flow rates, for the same residence time, which are desirable for higher power devices, or longer residence times for the same volumetric flow rates, which can potentially achieve greater conversion. The burner plates used in this burner are 3.2 mm thick.

For the small microcombustor, 3.2-mm-thick wall inserts composed of copper (k ~ 500 W/m·K) and type 316 stainless steel (k ~ 20 W/m·K) were tested. Experiments were also performed by removing the inserts and leaving a static air gap (k ~ 0.05 W/m·K) between the combustor wall and the insulation material. For the large microcombustor, a 3.2-mm-thick copper wall insert was used between the top plate of the microcombustor and the thermoelectric device. Additionally, a 3 cm-thick by 7 cm wide by 9 cm long finned aluminum heat sink was placed on top of the thermoelectric to act as a heat sink.

The catalytic inserts are formed by completely anodizing 75-μm-thick aluminum foil to create a large surface area alumina substrate. Figures 3 and 4 show the porous structure of the surface of the anodized alumina, which achieves a final thickness of ~ 100 μm. There exists a semi-ordered structure of pores, with approximately $2x10^{14}$ pores/m^2 of catalyst with diameters on the order of 50 nm. Approximately 1500 m^2 of surface area is exposed for every geometric m^2 of alumina resulting in approximately 14 m^2 per gram of catalyst. To deposit platinum catalyst, the alumina substrates are immersed in 0.007M aqueous dihydrogen hexachloroplatinate (IV) for 2 hours. The pH was modified, with sodium hydroxide or hydrochloric acid, to a value of 3. The acid was then reduced to platinum metal with H_2 at 600 ºC for 3 hours.
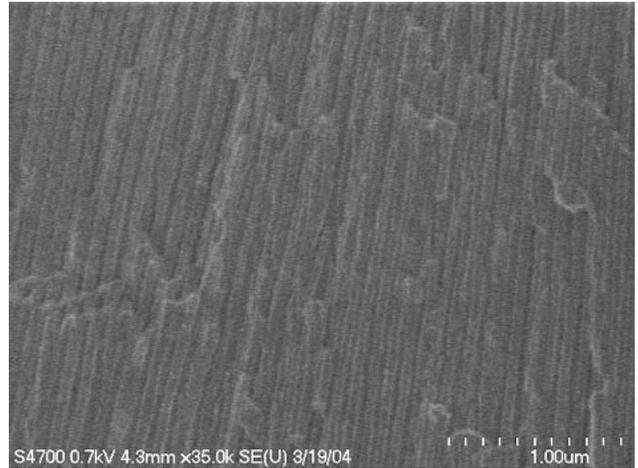

Figure 4. Scanning electron micrograph of the cross section of the pores in the anodized alumina. The pores start on either side of the wafer and meet at the center.

Thermocouples were spot welded to the exterior of the combustor walls, or placed under the insert and held in place with silver paste, to measure the temperature

profile. The thermocouples were attached in the middle of the channel, along the reactor. Since the reactor wall is very thin, these measurements provide reasonable estimates of the internal temperatures at those locations. During several trials, additional thermocouples were attached in the transverse direction, and good transverse temperature uniformity was observed. In addition, infrared (IR) imaging was used to interrogate spatial temperature profiles for un-insulated microcombustors.

Experiments are performed using hydrogen (H_2)/air and propane (C_3H_8)/air fuel systems. The feed flow and composition are controlled by mass flow controllers. For all experiments, the total flow rate is fixed at 2 standard liters per minute (SLPM), for ease of comparison between experiments. The exhaust gases are sampled with a gas sampling valve, and the composition is monitored with gas chromatography (GC), using both a thermal conductivity detector and a flame ionization detector.

The thermoelectrics used were Model HZ-2 from Hi-Z Technology, Inc. (San Diego, CA). The devices are approximately 2.9 cm wide × 2.9 cm long × 0.5 cm thick, weight 13.5 g, and are rated for output 2.5 W at 3.3 V.
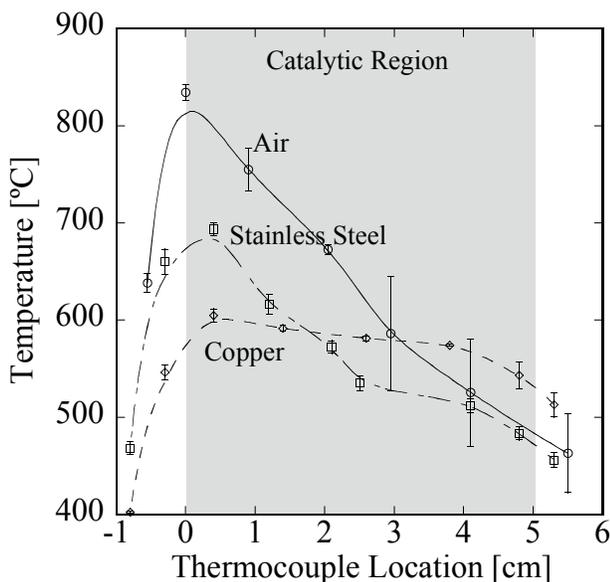
Figure 5. Temperature profiles for H_2/air combustion, with an equivalence ratio of 0.6, for different inserts. As the material conductivity increases, the temperature uniformity improves.

3. RESULTS

3.1 Thermal smoothing through materials modification

To efficiently utilize microcombustors with thermoelectrics, the temperature gradient across the thickness of the thermoelectric device must be maximized, while preventing the thermoelectric from being exposed to temperatures above the limits of its materials and packaging. These conditions require that controls exist for limiting the upper temperature of the microcombustor, and that uniform temperatures over the microcombustor device can be achieved. In this section we explore the effects of equivalence ratio, fuel type, and wall conductivity for achieving these objectives.
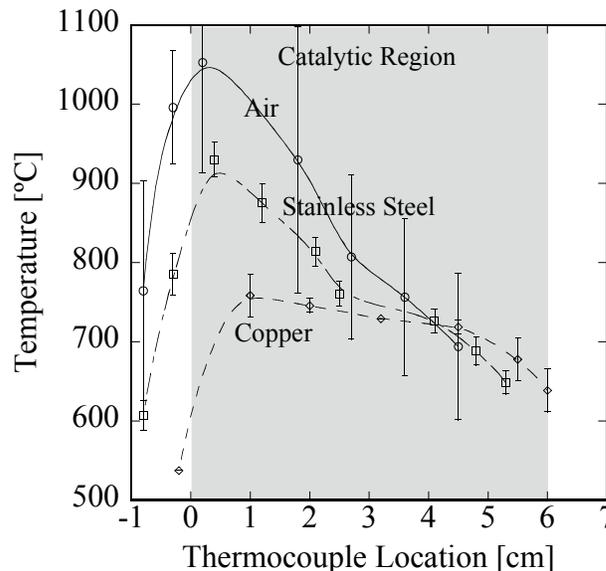
Figure 6. Temperature profiles for stoichiometric propane/air combustion, using different materials for the conducting inserts. As the material conductivity increases, the temperature uniformity improves.

Figure 5 shows the temperature profiles observed in the small microcombustor for H_2/air combustion at an equivalence ratio of 0.6 for the three types of wall inserts: copper, stainless steel, and air. The equivalence ratio is defined as the molar ratio of fuel to air normalized by the stoichiometric ratio of fuel to air. Figure 6 shows the corresponding temperature profiles for stoichiometric C_3H_8/air combustion. In both Figures the shaded region indicates the catalytic zone and the lines are smooth interpolations of the experimental points.

For both fuels, a sharp spike in temperature is observed at the start of the catalytic zone in burners with air inserts. As the flow continues downstream, wall temperature decreases. These profiles indicate that combustion occurs over a short length at the beginning of the catalytic zone. Once combustion is complete, cooling occurs due to heat losses. These heat losses include conductive losses which diffuse the thermal energy over the bulk of the metal device, as well as losses through the insulation material and into the environment. In the combustors with stainless steel inserts, the maximum temperature is decreased, and the temperature profile is slightly flattened. Finally, the temperature within the catalytic zone is nearly uniform when copper inserts are

employed. Note that the highest exit temperature is observed for the copper insert case, indicating that less heat is lost to the surroundings. However, the difference in exit temperatures for different conducting inserts is significantly smaller than the difference between the exit temperatures and the adiabatic flame temperatures. Therefore, the external reactor temperatures, and thus the external heat losses for all inserts are very similar.

Figure 7 shows the maximum temperature observed in the device as a function of equivalence ratio for both H_2 and C_3H_8 combustion for different conducting inserts. In general, the maximum temperature increases as the feed mixture tends towards stoichiometric (an expected result). For both fuels, as the thermal conductivity of the inserts increases, the maximum temperature decreases as a result of the thermal smoothing. H_2 combustion is stabilized down to the leanest possible limits, whereas C_3H_8 combustion extinguishes below an equivalence ratio of ~0.6. The equivalence ratio at which extinction occurs appears to be independent of the thermal conductivity of the insert. An important result from these experiments is that the maximum device temperature can be controlled by adjustment of the fuel/air ratio, with stable temperatures below 100ºC possible for very lean H_2 systems.
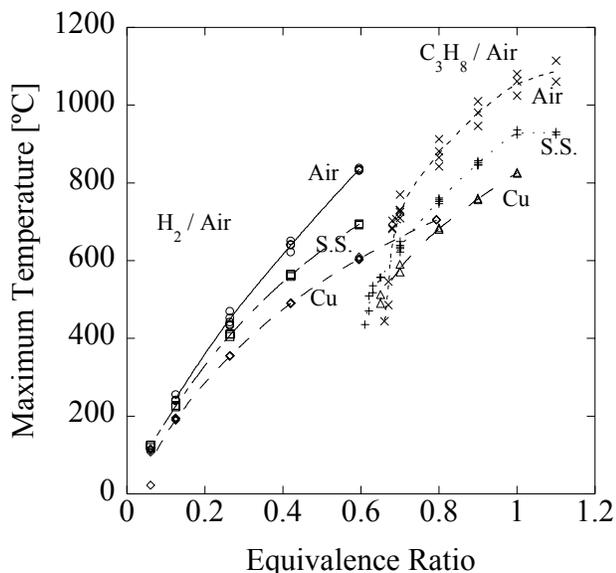

Figure 7. Maximum temperature measured in the microcombustor versus the equivalence ratio for H_2 and C_3H_8 combustion, for conducting inserts of different materials. H_2 allows stabilized combustion down to the leanest equivalence ratios. C_3H_8 extinguishes at an equivalence ratio of approximately 0.6, regardless of the conducting insert. S.S. stands for type 316 stainless steel. The lines are smooth interpolations of the experimental points.

Figure 8 shows the conversion of the fuel versus the equivalence ratio for both fuels for conducting inserts of different materials. For both fuels conversion is nearly

complete away from extinction, but some drop occurs for the leanest compositions. For the leanest compositions, the burner temperature drops significantly and reduces the reaction rate, such that incomplete combustion is observed. As nearly 100% chemical efficiency is achieved over a wide range of compositions for each fuel, these devices demonstrate great potential for efficient utilization of the combustion energy. Furthermore, GC measurements verify that, under these conditions, production of carbon monoxide or release of unburned fuel is very unlikely, enabling the use of these devices in close quarters with minimal safety concerns.
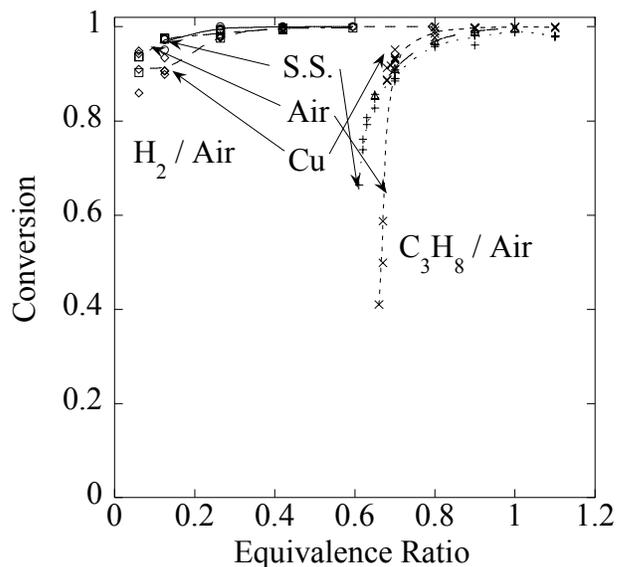

Figure 8. Conversion versus equivalence ratio for H_2 and C_3H_8 combustion, for conducting inserts of different materials. H_2 shows near complete conversion down to very lean compositions. C_3H_8 shows complete conversion down to near the extinction limit, where conversion drops off sharply. S.S. stands for type 316 stainless steel. The lines are smooth interpolations of the experimental points.

Figures 5 and 6 demonstrate that temperature uniformity is achievable using composite walls with exterior inserts made of highly conductive materials. However, as the equivalence ratio varies, so does the power generated. Therefore, it is important to assess that good temperature uniformity can be achieved for all compositions. Figure 9 shows the temperature differential, i.e., the difference between the maximum and minimum temperatures measured within the catalytic zone of the burner, as a function of equivalence ratio for H_2 and C_3H_8 combustion, for conducting inserts of different materials. Independent of the fuel and insert, as the equivalence ratio, and therefore the maximum temperature, increases, the temperature differential increases as shown in Figure 9. As expected, more conductive inserts decrease the temperature differential. For example, increasing the thermal conductivity from air to copper results in a decrease in the temperature differential by approximately

an order of magnitude. H_2 is able to self-sustain combustion at lower equivalence ratios and combust at lower temperatures than C_3H_8 combustion, and can therefore achieve lower temperature differentials.
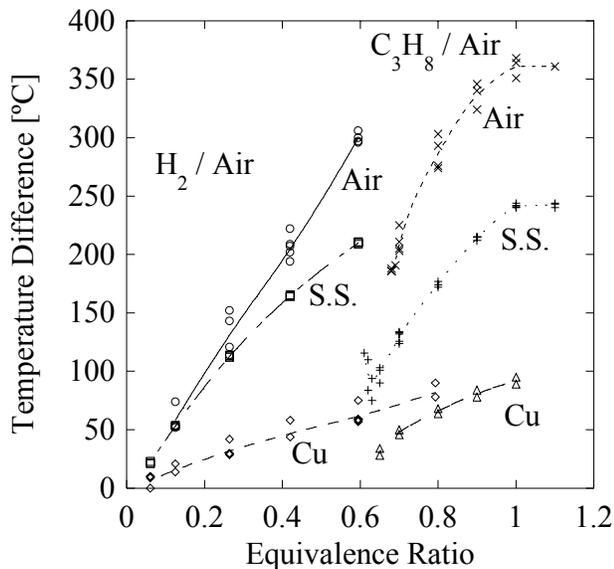

Figure 9. Temperature differential versus the equivalence ratio for H_2 and C_3H_8 microcombustion, for conducting inserts of different materials. Highly conductive walls reduce the temperature differential for both H_2 and C_3H_8 combustion. S.S. stands for type 316 stainless steel. The lines are smooth interpolations of the experimental points.

3.2 Thermal Imaging of Catalytic Microcombustors

In order to better understand the behavior of the catalytic microburners, thermal imaging using an IR camera was performed. During this procedure, the insulation was completely removed from all sides of the burner to enable the IR camera to directly view the microcombustor plates.

Figure 10 shows temperature contours for the catalytic microcombustion of H_2 in air, at an equivalence ratio of 0.6. The location of the internal catalytic insert is outlined for ease of visualization. There is good thermal uniformity in the transverse direction within the combustion channel, suggesting that the mixing screens are functioning adequately. Some transverse gradients are observable from the inner channel edge to the edge of the combustor plates. Hottest temperatures are observed shortly downstream of the inlet, with temperature then decreasing as the stream approaches the outlet. These axial temperature profiles are similar to those observed in Figures 5 and 6. This system is most similar to the air insert case; however, the IR and thermocouple measurements are not in quantitative agreement because of significant differences in insulation.

3.3 Power Generation from Integrated Catalytic Combustion-Thermoelectric Devices

In order to demonstrate the feasibility of generating electrical power from a catalytic microcombustor, the large microcombustor was coupled to a thermoelectric device as described in Section 2. For this device, maximum temperature can not exceed 250 ºC continuously or 400 ºC intermittently. In order to analyze the performance, the voltage drop and current were measured across different lengths of a nickel chromium resistive wire, for different fuels and various compositions. Runs using H_2/air and C_3H_8/air mixtures were stable over a range of equivalence ratios. However, the maximum temperatures for the C_3H_8/air system were beyond the maximum temperature limits of the thermoelectric device. For these systems, the thermal energy was further diffused by coupling the small microcombustor to the thermoelectric using a large copper wall insert sized for the large microcombustor. Under these conditions, thermal losses into the copper plate were so large that stable C_3H_8/air combustion could not be achieved. However, by inserting a thin layer of alumina insulation between the small microcombustor and the copper plate, stable C_3H_8/air combustion was achievable in the device.
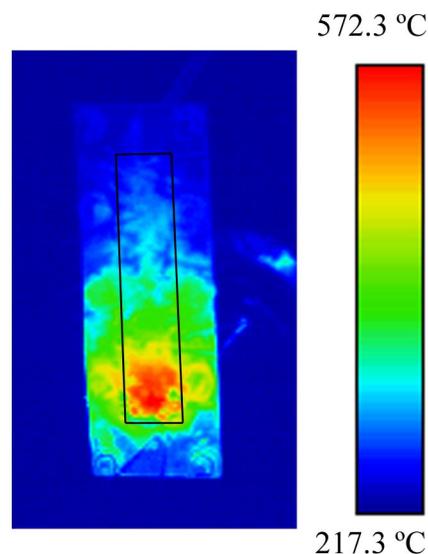

Figure 10. Infrared photograph of the microcombustor during combustion of H_2 / air at an equivalence ratio of 0.6. The location of the catalytic insert is outlined for ease of visualization.

Figure 11 shows the power generated versus the voltage supplied by the integrated thermoelectric–microcombustor device for H_2/air in the large microcombustor, and C_3H_8/air in the modified small microcombustor as described above. The data shown are for temperature differentials between the reactor and a heat sink of 253 ºC (H_2/air, equivalence ratio of $\phi = 1.0$),

206 ºC (H₂/air, ϕ = 0.60), 123ºC (C₃H₈/air, ϕ = 1.0), and 118 ºC (H₂/air, ϕ = 0.26). The maximum power achieved in these initial runs is approximately 1 W for stoichiometric H₂/air mixtures, representing approximately 1% thermal efficiency relative to the estimated 117 W of thermal energy being generated by the combustion reaction.

In order to test the performance of the thermoelectric-microcombustor devices under somewhat realistic conditions, they were used to power a portable electronic gaming device, a Gameboy® Advance, manufactured by Nintendo. The powered electrical leads from the thermoelectric were directly connected to the battery slot of the gaming device, as shown in Figure 12, which normally uses two AA batteries (for a total voltage of 3 V). Using the H_2 / air system at an equivalence ratio of ϕ = 0.42, the gaming device drew approximately 0.1 A at 2.5 V and functioned normally. Similarly, the device was also operated using C_3H_8 microcombustion at ϕ = 1.0.
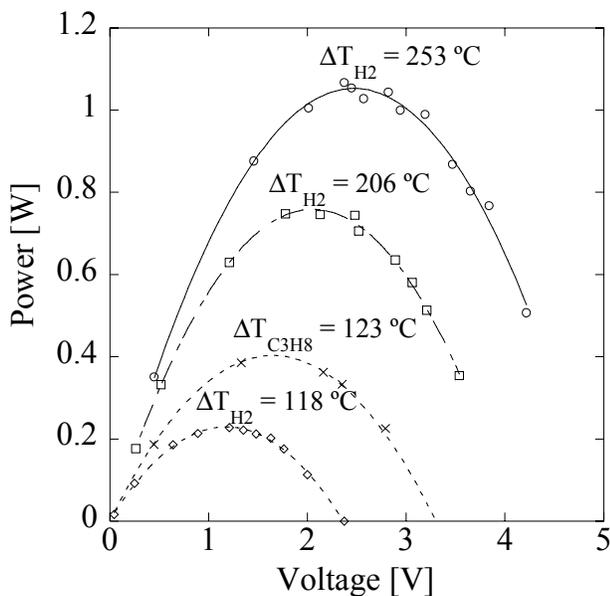

Figure 11. Power produced versus voltage supplied by the thermoelectric–microcombustor device for different differences in temperature between the reactor and heat sink and different fuels indicated.

To provide a conservative estimate of energy density for the thermoelectric–microcombustor device, we will assume a 100 g device with an additional 100 g of liquefiable hydrocarbon, such as propane. This mass of fuel is capable of producing 4700 kJ of thermal energy. Assuming 1% conversion efficiency to electricity and a total system mass of 200 g, the energy density of this system would be 0.24 MJ/kg. This value is comparable to the energy density of traditional batteries (0.5 MJ/kg) (Sitzki et al., 2001). Assuming a 1 W continuous load, such a device could operate for 13 hours from the 100 g fuel source. Higher efficiency values are possible if the

fuel-device mass ratio were increased. Efficiency and energy density increases are also possible, of course, through more careful engineering of the microcombustor and its packaging.
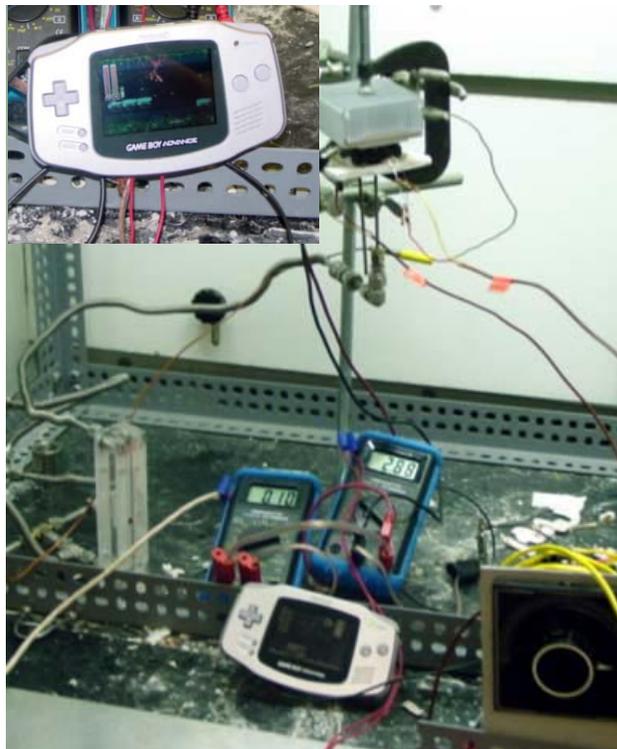

Figure 12. Photograph of a Gameboy® Advance being powered by a thermoelectric-microcombustor device. Inset: a close up of the device in action.

4. CONCLUSIONS

Compact catalytic microcombustors were fabricated to investigate the effect of axial thermal conductivity, fuel type, and fuel/air ratio on burner performance. These microcombustors have been shown to produce stable thermal energy over a broad range of temperatures and compositions for both H_2 and C_3H_8 combustion. Increasing the axial thermal conductivity of the wall materials greatly improves device thermal uniformity, without decreasing device stability. The H₂/air system offers lower combustion temperatures and allows leaner fuel/air mixtures, as compared with C_3H_8, demonstrating stable combustion temperatures below 100ºC. The C_3H_8 system, however, is simpler to implement due to the challenges associated with storing H_2 or reforming processes to produce H_2.

The feasibility of generating usable electrical power by coupling catalytic microcombustors with thermoelectric devices has also been demonstrated. Approximately 1 W of power was generated, at a thermal efficiency of ~1%, using both hydrogen and propane

systems. A portable consumer electronic device was powered by these microcombustors, demonstrating energy density comparable to batteries but utilizing hydrocarbon fuels. Continuing work in combustion efficiency, thermal management, packing materials, and fuel management should enable significant improvements in device performance and practicality.

REFERENCES

Ahn, J., C. Eastwood, L. Sitzki, K. Borer, and P. D. Ronney, 2003: Catalytic and noncatalytic combustion in heat-recirculating burners. *Proceedings of the Third Joint Meeting of the U.S. Sections of the Combustion Institute*, Pittsburgh, PA, E03.

Miller, J. A. and C. T. Bowman, 1989: Mechanism and modeling of nitrogen chemistry in combustion. *Progress in Energy and Combustion Science*, **15,** 287-338.

Norton, D. G. and D. G. Vlachos, 2004: Hydrogen assisted self-ignition of propane/air mixtures in catalytic microburners. *Proc. Comb. Inst.*, **30,** Accepted.

Norton, D. G., E. D. Wetzel, and D. G. Vlachos, 2004: Fabrication of single channel catalytic microburners: Effect of confinement on the oxidation of hydrogen/air mixtures. *Ind. Eng. Chem. Res.*, **43,** 4833-4840.

Patil, A. S., T. G. Dubois, N. Sifer, E. Bostic, K. Gardner, M. Quah, and C. Bolton, 2004: Portable fuel cell systems for America's army: technology transition to the field. *J. Power Sources*, **In Press**.

Schaevitz, S. B., A. J. Franz, K. F. Jensen, and M. A. Schmidt, 2001: A combustion-based MEMS thermoelectric power generator. *The 11th International Conference on Solid-State Sensors and Actuators*, Munich, Germany.

Sitzki, L., K. Borer, E. Schuster, P. D. Ronney, and S. Wussow, 2001: Combustion in Microscale Heat-Recirculating Burners. *The Third Asia-Pacific Conference on Combustion*, Seoul, Korea.